THE PENNSYLVANIA STATE UNIVERSITY
SCHREYER HONORS COLLEGE

DEPARTMENT OF CHEMICAL ENGINEERING

POLYMERIZATION-INDUCED NANOSTRUCTURAL TRANSITIONS DRIVEN BY IN SITU POLYMER GRAFTING FOR DIBLOCK COPOLYMER AND MONOMER BLENDS

EVERETT ZOFCHAK

SPRING 2019

A thesis
submitted in partial fulfillment
of the requirements
for baccalaureate degrees
in Chemical Engineering and Materials Science and Engineering
with honors in Chemical Engineering

Reviewed and approved* by the following:

Robert J. Hickey III
Assistant Professor of Materials Science and Engineering
Thesis Supervisor

Manish Kumar
Associate Professor of Chemical Engineering
Thesis Supervisor

Scott T. Milner
Joyce Chair Professor of Chemical Engineering
Honors Adviser

R. Allen Kimel
Associate Teaching Professor of Materials Science and Engineering
Honors Adviser

* Signatures are on file in the Schreyer Honors College.

ABSTRACT

Nanostructured polymeric materials have attracted the interest of researchers in recent years for their use in a vast array of technologically relevant applications. One common method of creating nanostructured polymer materials is through diblock copolymer self-assembly, which occurs due to the microphase separation of two chemically distinct polymers covalently attached at a single point. The phase behavior of linear diblock copolymers has been exhaustively researched, yet less well understood is how selective polymer grafting from one block of a diblock copolymer effects the mesoscale ordering of the system. The work presented in this thesis illustrates how polymerization-induced nanostructural transitions can be achieved via in situ polymer grafting from the diblock copolymer poly(styrene)-*block*-poly(butadiene) (PS-PBD). Emphasis will be placed on the determination of the resultant static morphology after removal of residual monomer and annealing, the dominant grafting mechanism at play, and the in situ characterization of these nanostructural transitions. Through this in situ grafting process lamellar, hexagonally packed cylinders, and disorder spheres structures have been achieved as the final static dried and annealed morphology, as determined by small-angle X-ray scattering (SAXS) and transmission electron microscopy (TEM). In addition to the static phase behavior, the phase behavior of blends of diblock copolymer and monomer was monitored via in situ SAXS and rheology experiments during polymerization. The in situ measurements revealed an interesting and unexpected phase trajectory for the 60% PS-PBD and 40% styrene monomer by volume blend. This thesis outlines our current knowledge regarding the phase behavior of these nanostructured polymeric materials made via in situ polymer grafting, as well as the limitations of this method and future work in this arena of research

TABLE OF CONTENTS

LIST OF FIGURES

ACKNOWLEDGEMENTS

First and foremost, I would like to express my deepest gratitude to Dr. Robert Hickey for allowing me the opportunity to work and learn in his lab over these past few years. Conducting research in your lab has had a profound impact on my career trajectory and has given me a truly unique and fulfilling undergraduate research experience. You have afforded me many enriching opportunities that have guided me to where I am today, and I had a lot of fun along the way. For your mentorship I am forever grateful.

I would also like to thank graduate student Jake LaNasa for the incalculable hours of time he spent assisting me with my research. He played an integral role in the numerous SAXS experiments littered throughout this thesis and trained me on several of the instruments/ techniques that were central to my research.

None of this work would be possible without the support of the PPG/MRI Undergraduate Research Fellowship and the Penn State Erickson Discovery Grant. I am also thankful for the assistance of Materials Characterization Lab faculty members Missy Hazen and Nichole Wonderling for their help staining and microtoming polymer samples for TEM and setting up SAXS experiments, respectively. Additionally, thank you to Dr. Chao Lang for taking the TEM images and graduate student Joshua Bostwick for collecting rheology data.

Lastly, I would like to thank my family and friends for helping to keep me relatively sane throughout my undergraduate career. My parents, brother, and sister have been a terrific support system and have stood by me through all my academic and personal endeavors. I am grateful for my friends and their sustained but necessary supply of distractions and laughs that have kept me in good spirits.

DEDICATION

This thesis is dedicated to my family and friends.

Chapter 1: Introduction

1.1 Motivation

Polymerization-induced structural transitions have recently gained attention due to the ease with which one can create materials with controlled morphologies and length scales. Materials made via polymerization-induced transitions are ubiquitous and span across multiple technological applications, including but not limited to polymersomes for drug delivery,[1] high-modulus batteries,[2] and structural materials, such as high-impact poly(styrene) (HIPS) and acrylonitrile-butadiene-styrene (ABS) plastics.[3-5] HIPS and ABS differ from other common polymerization-induced structural transitions, namely polymerization-induced self-assembly (PISA) and polymerization-induced microphase separation (PIMS), in that HIPS and ABS leverage grafting of monomer from poly(butadiene) (PBD) to induce the phase separation that leads to their intricate phase behavior.[1-5]

Molecular architecture is an important parameter that dictates the final morphology of self-assembled macromolecules. Well-defined complex polymer architectures such as graft, bottlebrush, and miktoarm star polymers exhibit fascinating phase behavior that depend on several parameters; however, less well established is the exploitation of in situ polymer grafting to tune the resultant nanostructure of a material. By utilizing in situ grafting, linear block copolymers can be converted into polymers with complex architectures, allowing one to access a plethora of thermodynamic structures from a single block copolymer. From a scientific standpoint, the ability to essentially “tune” the standard thermodynamic phase space of

linear block copolymers to resemble the more intricate phase space of multiblock polymers with complex architectures opens the door to an array of new and exciting fundamental studies on the relationship between molecular architecture and mesoscale assembly that are not currently possible. In addition to being scientifically interesting, polymerization-induced structural transitions are industrially practical, as polymers with graft architectures are commonly found in commercial applications. Since the properties of polymeric systems are intimately tied to their underlying structure,[6] understanding how grafting effects the underlying morphology is paramount to creating new soft materials with novel properties.

1.2 Background

The bulk of the work presented in this thesis is concerned with the phase separation of multiblock polymer systems with complex molecular architecture. It is useful, however, to first understand the thermodynamic origins of phase segregation in the simplest case – mixing of two chemically distinct homopolymers. Flory-Huggins solution theory adequately describes the Gibbs free energy of mixing (ΔG_m) of two chemically distinct homopolymers (A and B) by accounting for their volume fractions, φ, degree of polymerization, N, their Flory-Huggins interaction parameter, χ, and the Boltzmann constant and absolute temperature, k and T, respectively.[7] Negative free energies of mixing correspond to spontaneous and favorable mixing, while positive values correspond to unfavorable mixing, and therefore phase separation (like oil and water).

$$\frac{\Delta G_m}{k\,T} = \frac{\varphi_A}{N_A} ln\varphi_A + \frac{\varphi_B}{N_B} ln\varphi_B + \varphi_A \varphi_B \chi \quad (1.1)$$

The Flory-Huggins interaction parameter reflects the enthalpic nature of the interactions between polymer chains, and to some extent an excess entropy of mixing. The Flory-Huggins parameter can be approximated using classical solution theory, but that approximation is often rough and fails to allow for negative values of χ. Instead, the empirical relation shown in Eq 1.2 is often employed, where α and β are experimentally determined parameters.

$$\chi = \frac{\alpha}{T} + \beta \quad (1.2)$$

Nonetheless, χ is typically a small positive number, indicating that for most polymer-polymer mixtures the enthalpic interactions are unfavorable and thus a barrier to homogenous mixing. For spontaneous mixing to occur, the entropic contributions (represented by the logarithmic terms in Eq 1.1) must drive the free energy to be negative. These entropic terms are always negative, as $0 < \varphi_i < 1$ and $ln\varphi_i \leq 0$; however, they are confounded by their inverse relationship to the degree of polymerization for each respective polymer species. Degrees of polymerization frequently range from 10^2 for modest polymers to 10^6 for larger ones, and thus the magnitude of the entropy of mixing is appreciably diminished even for relatively small polymers. Therefore, the tendency for polymer blends to macrophase separate is predominantly a consequence of the entropic penalty associated with mixing large, chain-like molecules.

The tendency for phase separation is both a blessing and a curse as it complicates recycling and polymer processing, yet has profound implications for technological applications, particularly in the fields of nanotechnology. Block copolymers (BCPs), which are two chemically distinct polymers tethered together via a covalent bond, leverage similar physics to homopolymer phase separation, but they are topologically connected and are therefore unable to completely phase

separate from one another. BCPs instead undergo *microphase separation* into an array of thermodynamic nanoscale morphologies, as shown in Figure 1. The morphology of the BCP is dictated by the competition between the enthalpic driving force to phase separate and the entropic penalty associated with chains stretching away from their equilibrium random-walk conformation and the local alignment of block-block connections at an interface.[7]

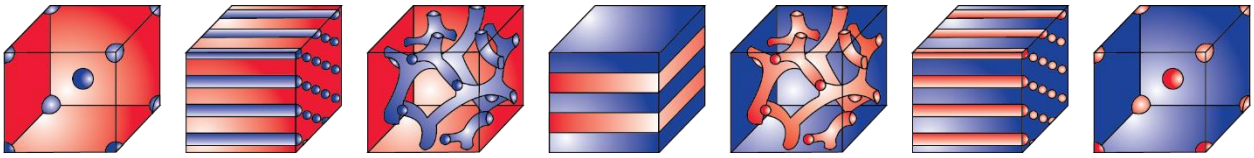

Figure 1. Thermodynamic phases of BCPs, with increasing volume fraction of "blue" polymer from left to right. Body-centered spheres (BCC), hexagonally-packed cylinders (HEX), gyroid (GYR), and lamellar (LAM) phases are shown (left to right), though other complex phases exist.

The thermodynamic morphologies displayed in Figure 1, which are typically characterized via small angle x-ray scattering (SAXS) and transmission electron microscopy (TEM), are all accessible by varying three parameters: volume fraction of block A (f_A), the total volumetric degree of polymerization (N), and the Flory-Huggins interaction parameter, χ. Microphase separation in these systems is quantified by the product of the Flory-Huggins interaction parameter and the degree of polymerization, χN, and leads to the construction of the somewhat universal phase diagram shown in Figure 2. For $\chi N << 10.5$ entropy drives neat volumetrically symmetric BCP systems toward homogeneity, where no periodic structure exists. When $\chi N \approx 10.5$, entropic and energetic factors balance each other, allowing the ordered mesophases displayed in Figure 1 begin to form. For $\chi N >> 10.5$, energetic factors dominate and ordered morphologies with sharp interfaces begin to arise. Figure 2 also shows that as f_A deviates away from volumetric symmetry ($f_A = 50\%$), the requisite χN for phase segregation increases and the curvature at the BCP interface increases.[7]

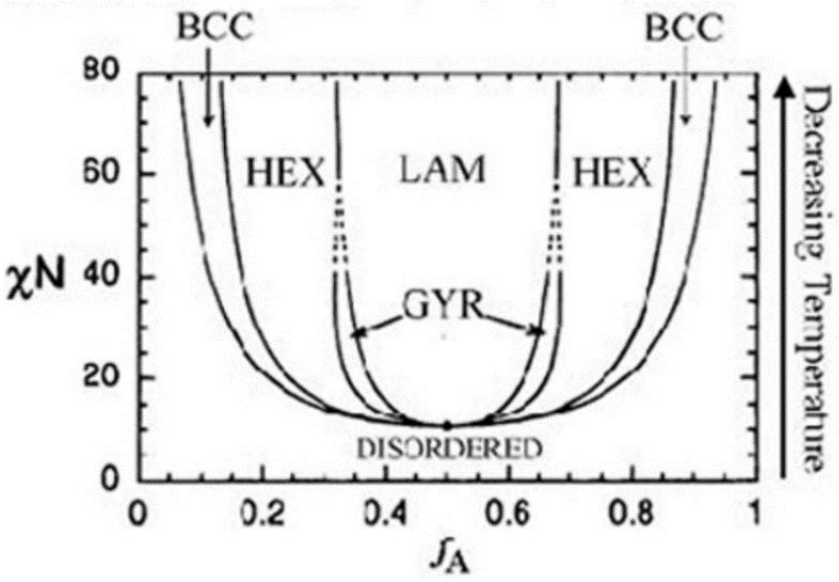

Figure 2. Universal phase diagram for AB diblock copolymers.[25]

While the physics described above explains the microphase separation behavior of diblock copolymers, a similar explanation can be used to describe PISA and PIMS. In these two methods, starting reagents, macro chain-transfer agents (macro-CTA), monomer and solvent are initially homogenously dispersed in solution. As the polymerization progresses through the macro-CTA chain extension process, the nascent polymer chain becomes incompatible with the initial polymer segment and/or solvent, thus producing well defined nanoscale domains. With these methods a variety of other ordered structures can be accessed, ranging from polymersomes to disordered co-continuous nanochannels. These different structures are targeted depending on their desired applications and can be achieved by precise control over monomer chemistry and polymerization conditions.

Macromolecular architecture is yet another parameter that profoundly effects the resultant nanoscale morphology of block copolymers. Nonlinear architectures such as graft, bottlebrush, and miktoarm star exhibit remarkably intricate phase behavior that, like standard BCPs, can be tuned via independent control over χ, N, and f. In these complex architecture block copolymer

systems, well defined polymers are typically studied and less well-defined (and in turn, synthetically simplistic) procedures are jettisoned for more controlled methods. In situ polymer grafting has the potential to control the final morphology, and thus properties, of a two-polymer system, but is currently not well studied or understood. The most common example of exploiting in situ polymer grafting to control morphology arises in HIPS production, in which polybutadiene (PBD) is dissolved in styrene monomer with initiator. Upon thermal initiation, polystyrene grafts from the PBD and leads to a final complex morphology of rubbery PBD droplets in a PS matrix. The remarkable impact resistance of HIPS is derived from the properties of both PBD and PS, as well as the final morphology of the system, which is determined by graft number, graft length, and graft density.

In this thesis, the phase behavior of ternary blends of PS, PBD and polystyrene-*block*-polybutadiene (PS-PBD) block copolymers is presented along with the phase behavior of PS-PBD-*graft*-PS (PS-PBD-g-PS) made via in situ polymer grafting from the PBD block of PS-PBD. SAXS and TEM data are presented and reveal a complex phase space and interesting order-order and disorder-order transitions. The chemical mechanism by which grafting occurs is hypothesized and discussed in the context of PBD microstructure. Future work to further elucidate the dominant chemical grafting mechanism is proposed.

Chapter 2: Synthesis and Characterization of Materials and Blends

2.1 Living Anionic Polymerization and Characterization of PS-PBD, PBD, and PS

Living anionic polymerization is a living chain growth synthesis method capable of producing a diverse array of polymers with incredibly narrow molecular weight dispersities ($Đ$).

The low dispersity ($Đ \approx 1$) is attributed to the so-called "living" nature of the propagating polymer chain. After the rapid initiation of the polymerization with a hot nucleophile, such as organo-lithium compounds, propagation takes place and continues until all monomer in solution has been exhausted or a terminating agent, such as methanol, has been added to the reaction mixture.

The polystyrene-*block*-polybutadiene (PS-PBD) diblock copolymer used in this thesis was synthesized via sequential living anionic polymerization. Monomer purification and reactor set up have been previously reported and are well-established procedures.[8] Styrene and 1,3-butadiene monomer were purified twice over di-*n*-butylmagnesium and *n*-butyllithium, respectively, before initiation with *sec*-butyllithium. Solvents used for anionic polymerizations, tetrahydrofuran (THF) and cyclohexane (CHX), were purified using solvent columns (JC Myer). Methanol (Fischer Scientific) and benzene (Fischer Scientific) were used for precipitation and freeze-drying of the polymerization product, respectively. PS-PBD with a 1,2 microstructural

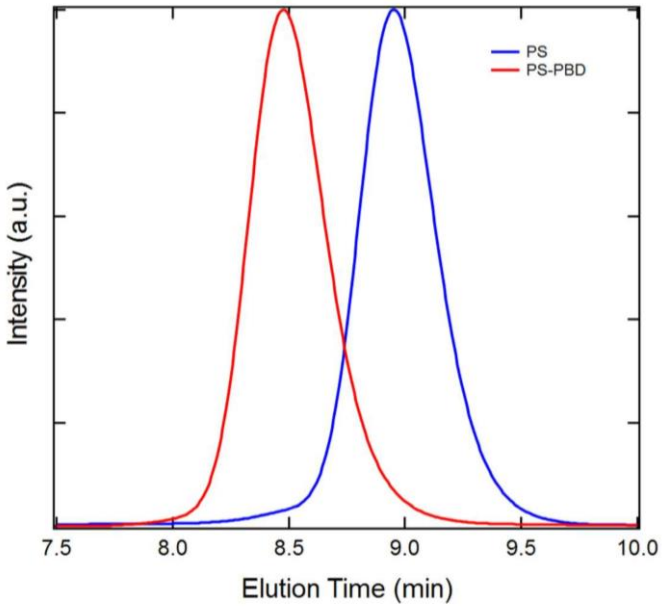

Figure 3. SEC chromatograms of the homopolymer PS aliquot obtained prior to addition of 1,3-butadiene and the resulting PS-PBD diblock copolymer.

content of roughly 90% was targeted by adding a THF/*sec*-butyllithium molar ratio of 100:1, as established in previous synthetic procedures.[9] Styrene was first polymerized in pure cyclohexane at 40°C for 4 /h, after which an aliquot was taken to determine the number-average molecular weight (M_n) and $Đ$ of the PS blocks (Figure 3).

After the initial 4 h polymerization of PS, the reaction mixture was cooled to ~ 5°C using an ice-water bath. THF was then added to ensure ~90% 1,2 addition after the addition of 1,3-butadiene. The reaction proceeded for 4 additional h and was then terminated with degassed methanol. The M_n, volume fraction of PS block (f_{PS}), $Đ$, and 1,2/1,4 microstructural content was determined to be 27.5 kg/mol, 0.58, 1.03, and 0.94, respectively. Volume fractions and molecular weights were determined via multi-angle light scattering in tandem with size-exclusion chromatography (SEC) and room temperature densities of 1.04 g/mL and 0.86 g/mL for PS and PBD homopolymers (densities from Sigma-Aldrich). The fraction of 1,2 addition ($\varphi_{1,2}$) in the PBD block was determined using a Bruker AVIII-HD 500 MHz ^{1}H NMR (Figure 3).

1,2 PBD homopolymer (M_n = 20.33 kg/mol, $Đ$ = 1.04, $\varphi_{1,2}$ = 0.9) was also synthesized via living anionic polymerization at similar conditions used for the PBD block in the PS-PBD synthesis. A solution of THF and CHX was cooled to ~5 °C in an ice-water bath before charging with *sec*-butyllithium and purified 1,3-butadiene, sequentially. The reaction was terminated after 4 h with degassed methanol and was characterized via SEC and 400 MHz ^{1}H NMR (Figure 5).

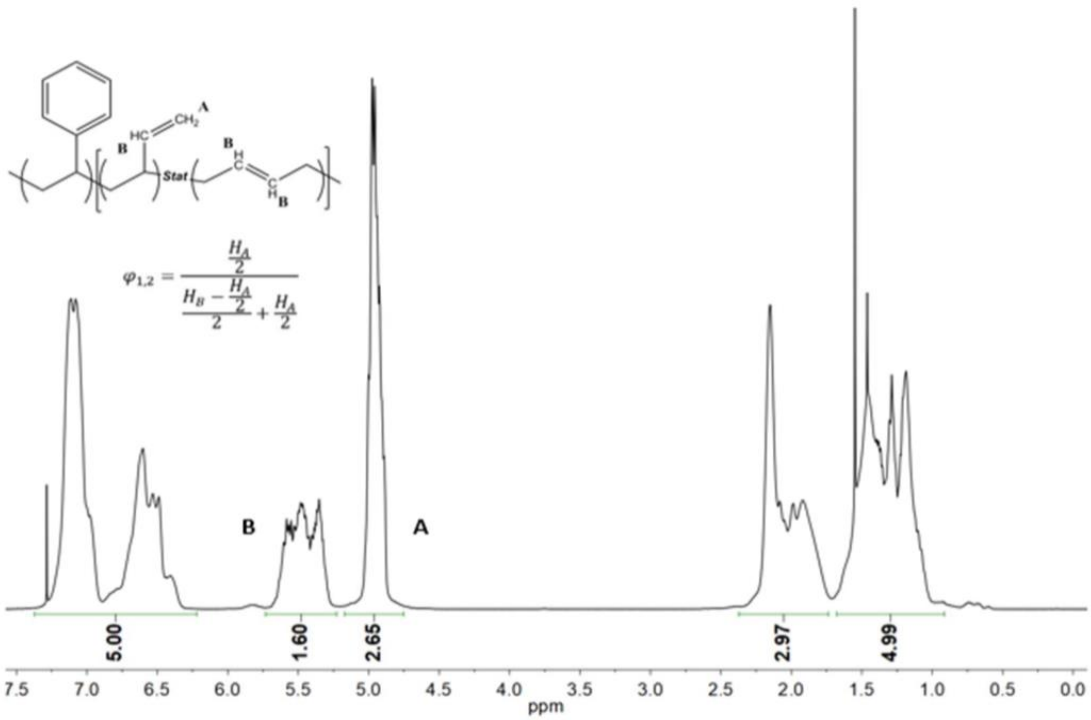

Figure 4. 500 MHz 1H NMR spectra for PS-PBD synthesized via sequential living anionic polymerization. Within the spectra is the equation used to determine fractional 1,2 content.

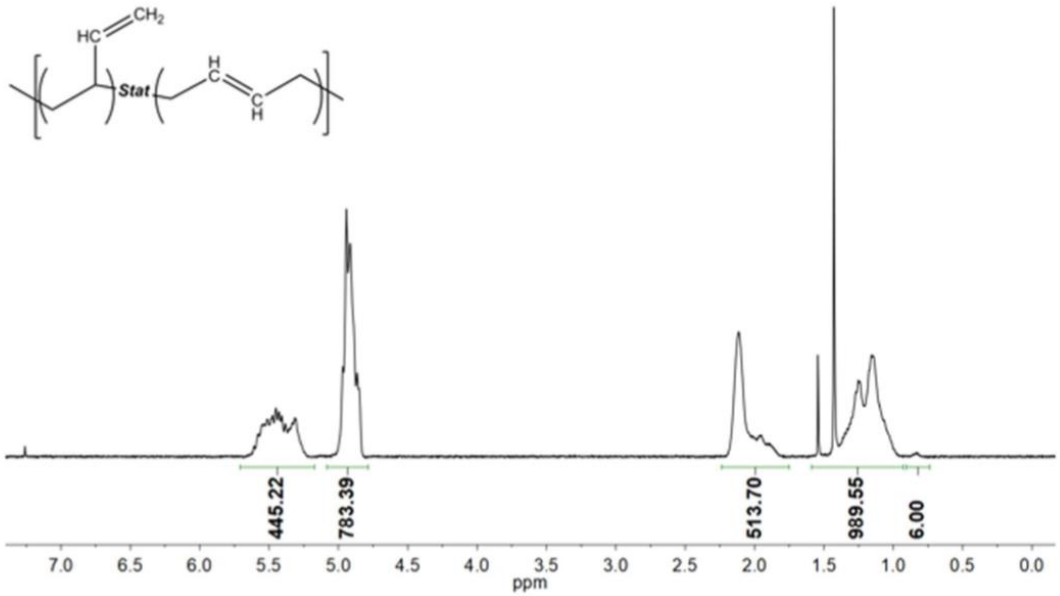

Figure 5. 400 1H NMR spectra of PBD synthesized via living anionic polymerization**.**

PS homopolymer (M_n = 6.1 kg/mol, $Đ$ = 1.03) was synthesized via anionic polymerization of styrene at 40 °C in CHX.

Small-angle X-ray scattering (SAXS) measurements on the neat PS-PBD diblock copolymer were performed at the Penn State Materials Characterization Lab using Cu K_α radiation source from a Xeuss 2.0 beamline (Xenocs) installed with a Pilatus3R 200K-A detector (Dectris). Incident x-rays had a wavelength of 1.54 Å and an energy of 8.05 keV. Calibration of q, the scattering wavevector, was performed using powdered silver behenate.

The neat PS-PBD was scanned as a bulk film approximately 1.5 mm in thickness. Figure 6 shows the resultant scattering pattern of the film at room temperature. The scattering pattern indicates that the film has a lamellar morphology due to q/q^* indexing to integer whole numbers. The presence of evenly indexed peaks ($q/q^* = \sqrt{4}$ and $\sqrt{16}$) suggests that the lamellae are asymmetrical, a result that is expected for a lamellar block copolymer with volumetrically asymmetrical blocks (f_{PS} = 0.58). Higher order reflections ($q/q^* = \sqrt{16}$ and $\sqrt{25}$) indicate long range order in the bulk film. The domain spacing was found to be approximately 25 nm using Eqn. 2.1.

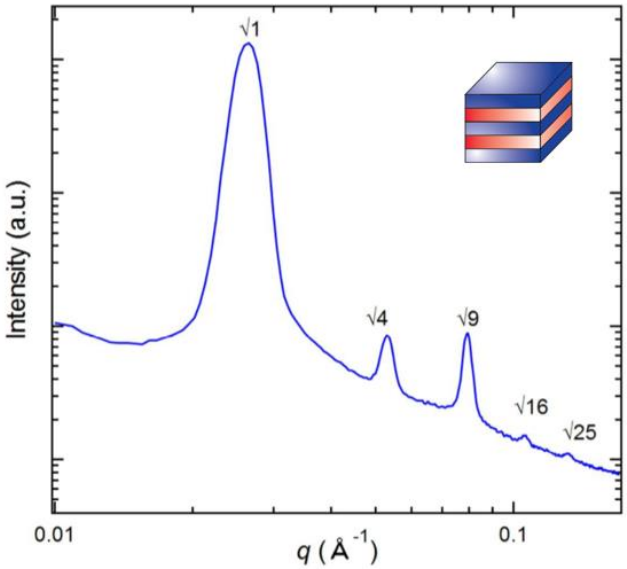

Figure 6. Room temperature SAXS pattern for the neat PS-PBD after annealing under vacuum at 100 °C overnight.

$$d = \frac{2\pi}{q^*} \quad (2.1)$$

2.2 Nitroxide-Mediated Polymerization of Styrene

Nitroxide-mediated radical polymerizations (NMP) are a form of controlled living radical polymerization utilizing stable radical alkoxyamines to control the kinetics of the reaction. Controlled living radical polymerizations - including but not limited to NMP - operate on the establishment of a dynamic equilibrium between a dormant radical species that cannot propagate and a free radical which can propagate. NMP reactions specifically rely on the addition of an alkoxyamine to a macroradical, which renders the nascent chain dormant, and subsequent homolytic cleavage of the bond yielding a propagating chain. For the reaction to be controlled the equilibrium of the reaction must favor the dormant state, thus allowing only a few monomers to add to the chain at a time and slowing the overall rate of polymerization. [10]

PS homopolymer was synthesized in bulk using NMP with initiator systems consisting of (i) benzoyl peroxide (BPO, Sigma-Aldrich, 98%) and (ii) 2,2'-Azobis(2-methylpropionitrile (AIBN, Sigma-Aldrich, 98%) with 4-hydroxy-2,2,6,6-tetramethylpiperidine (OH-TEMPO, Sigma-Aldrich, 97%). Inhibitor was removed from styrene monomer (Sigma-Aldrich, >99%) by flowing through a column packed with basic alumina ($Al(OH)_3$, Sigma-Aldrich) A typical PS reaction procedure consisted of dissolving 14.2 mg of BPO (0.058 mmol) and 6.7 mg of OH-TEMPO (0.0389 mmol) with 1 mL of styrene and polymerizing for 3 h at 125 °C. The reaction mixture was then dissolved in THF, precipitated in methanol, and dried in vacuum at 80 °C overnight (M_n = 14.1 kg/mol, $Đ$ = 1.34, ~ 70% yield). AIBN PS was synthesized using the same molar values as described above (M_n = 8.62 kg/mol, $Đ$ = 1.54). SEC traces for both polymerization procedures are shown in Figure 7.

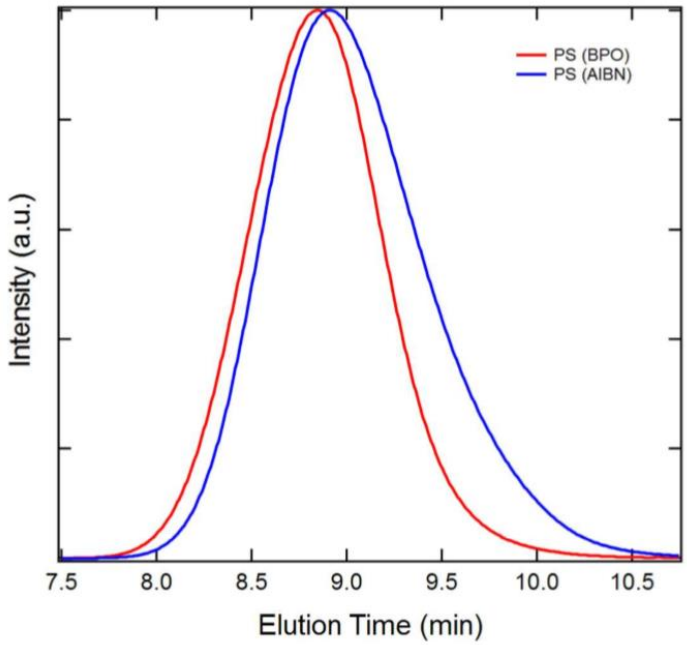

Figure 7. SEC traces for NMP polymerizations of PS using AIBN (blue) and BPO (red)

Polymerizations were run using microwave heating and conventional heating processes. Both procedures produced polymers that were indistinguishable from one another and were thus used interchangeably. Microwave induced polymerizations were run using a Discover LabMate with IntelliVent pressure and infrared temperature control system (CEM Co.) in dynamic power mode at 100 W, 125 °C, with a 20 °C/min temperature ramp.

2.3 PS-PBD/ Styrene Preparation

PS-PBD/styrene, 1,2PBD/styrene, and PS/styrene blends were prepared by dissolving the polymer of interest in a styrene solution containing the same molar ratios of BPO to OH-TEMPO to styrene outlined in section 2.2. A typical blending procedure for a 60% volume PS-PBD and 40% volume styrene solution consisted of combining 0.522 g of PS-PBD with 0.4 mL of styrene/BPO/TEMPO solution. Blends were then heated to 65 °C for approximately 15 min and agitated to promote homogeneous mixing. Reaction conditions for PS-PBD/styrene, PBD/styrene, and PS/styrene blends were identical to the conditions used for microwave PS homopolymer synthesis.

Chapter 3: Polymerization-Induced Nanostructural Transitions

3.1 Order-Order and Disorder-Order Transitions

Order-order (OOT) and order-disorder (ODT) transitions commonly occur in diblock copolymers.[11] These transitions are generally governed by changing the product χN, via temperature or pressure differences, which leads to crossing of a phase boundary. Referencing

the phase diagram in Figure 2 for a LAM forming diblock copolymer at f_A = 0.5, increasing temperature will decrease χ (Eq. 1.2) and cause χN << 10.5, thus leading to a disordered diblock copolymer melt via an ODT. Similarly, for a diblock copolymer of f_A = 0.65 and χN = 20, increasing temperature will lead to an OOT from GYR to HEX.[12]

ODTs and OOTs have also been observed in PS-PBD/Styrene blends upon polymerization. Figure 8 illustrates OOT and ODT in 60/40 and 40/60 PS-PBD/Styrene blends, respectively. In addition to the LAM-to-HEX and DIS-to-HEX transitions observed in $\phi_{PS\text{-}PBD}$ = 60% and $\phi_{PS\text{-}PBD}$ = 40% blends, transitions from DIS to disordered spheres has also been observed. The DIS-to-DIS spheres transitions occurred for blends consisting of $\phi_{PS\text{-}PBD}$ = 20%, shown in Figure 9. For each of the observed polymerizations, approximately 70% conversion was obtained.

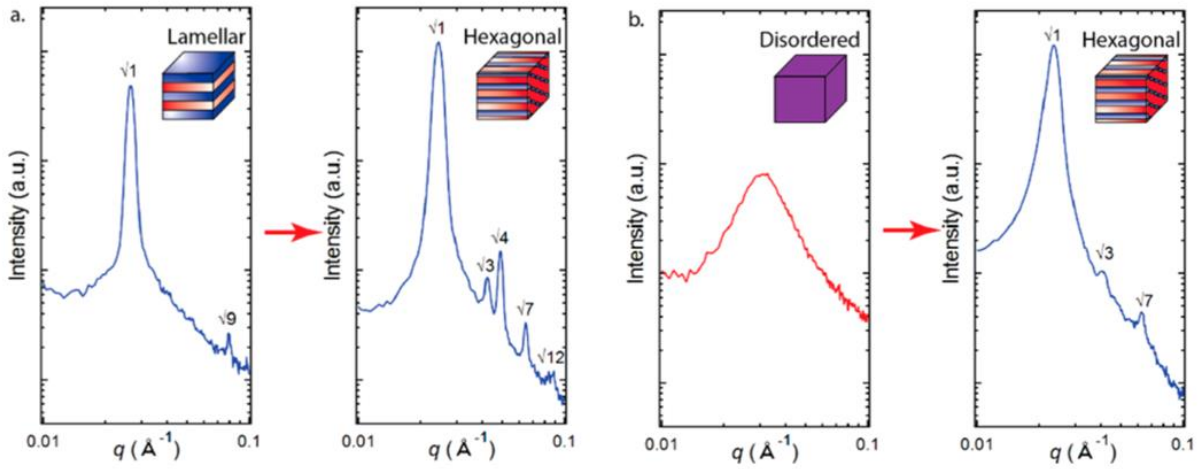

Figure 8. Room temperature 1-D SAXS patterns for the polymerization induced morphology transitions. Red arrows lead to the morphology after polymerization. (a) Lamellar-to-hexagonal ($\phi_{PS\text{-}PBD}$ = 60%) and (b) disorder-to-hexagonal ($\phi_{PS\text{-}PBD}$ = 40%) transitions were observed.

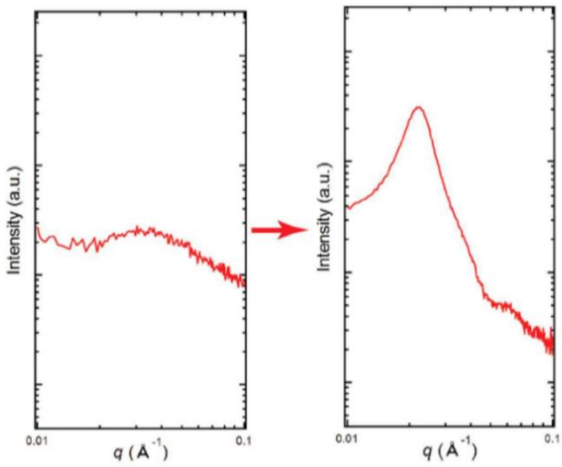

Figure 9. DIS-to-Spheres transition observed for $\phi_{PS\text{-}PBD}$ = 20%. The post-polymerization SAXS pattern right of the red arrow is characteristic of scattering in a disordered sphere system.

3.2 Phase Behavior of Dried Blends

Once polymerized, blends were dried and annealed under vacuum at 125 °C for 36 to 48 h. This was done to ensure that the structures observed were not swollen with residual styrene monomer and that the observed structure was thermodynamically stable. Room temperature SAXS patterns are displayed below in Figure 10 A-F.

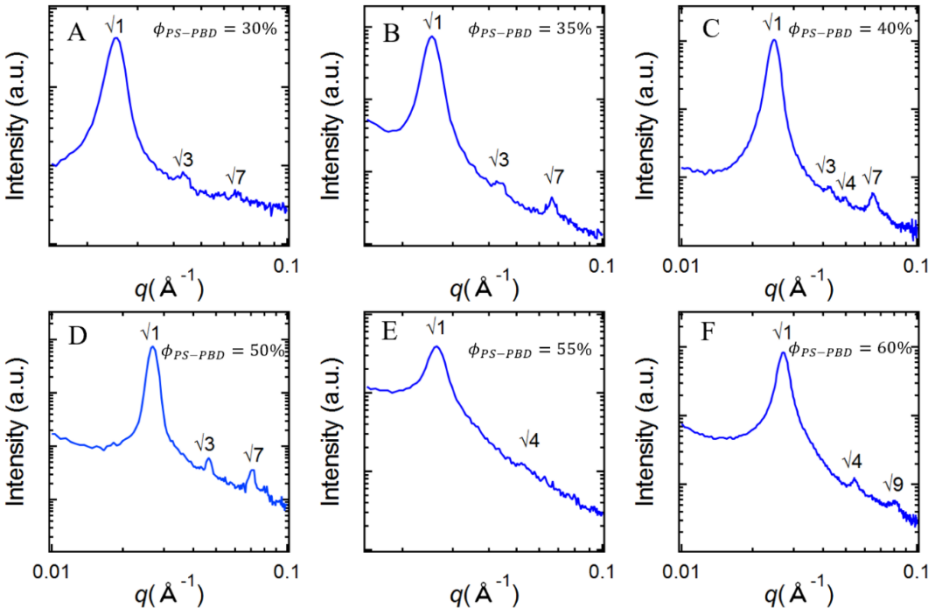

Figure 10. Annealed SAXS patterns for ordered blends post polymerization (A) $\phi_{PS\text{-}PBD}$ = 30%, (B) $\phi_{PS\text{-}PBD}$ = 35%, (C) $\phi_{PS\text{-}PBD}$ = 40%, (D) $\phi_{PS\text{-}PBD}$ = 50%, (E) $\phi_{PS\text{-}PBD}$ = 55%, and (F) $\phi_{PS\text{-}PBD}$ = 60%.

Indexing of the SAXS patterns in Figure 10 suggest that DIS spheres, HEX, and LAM mictrostructures were obtained after polymerization of PS-PBD/ Styrene blends. These nanostructures are summarized in Figure 11.

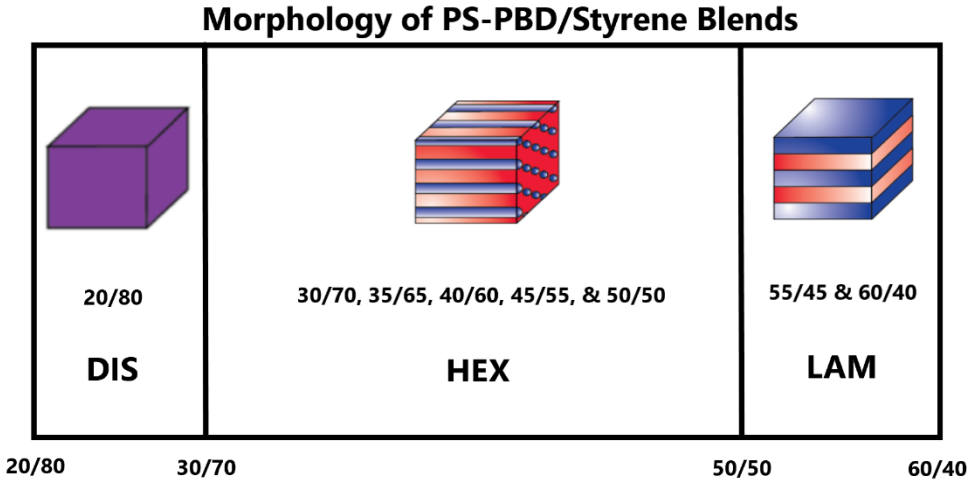

Figure 11. Phase behavior for polymerized blends of PS-PBD and Styrene after drying and annealing.

TEM images were taken for select blends to confirm their mesoscale structure (Figure 12). Dark regions are OsO_4 stained PBD, which selectively stains the double bonds in PBD but not the aromatic rings in PS. The LAM, HEX, and DIS morphologies shown in the TEM images agreed with the structure determined via SAXS.

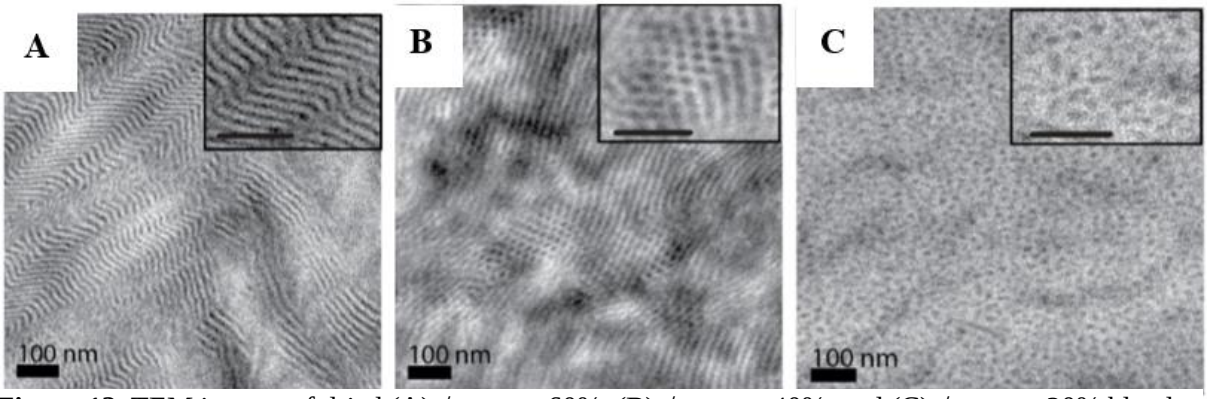

Figure 12. TEM images of dried (A) $\phi_{PS\text{-}PBD}$ = 60%, (B) $\phi_{PS\text{-}PBD}$ = 40%, and (C) $\phi_{PS\text{-}PBD}$ = 20% blends. Samples were cryosectioned into 70 – 90 nm films (Leica UC6 ultramicrotome w/ FC6 cryo-attachment) and stained with OsO4 for 15 min. Imaging performed on FEI Tecnai G2 Spirit BioTwin TEM

Next, the static morphology of the dried blends was compared to blends of similar compositions of PS-PBD and PS. A ternary phase diagram of PS, PBD, and PS-PBD was generated by freeze drying blends of anionically synthesized diblock and homopolymers in varying volume fractions (Figure 13). The right leg of the diagram illustrates the resultant morphology of binary blends of PS-PBD and PS, with 100 vol % PS-PBD at the top of the diagram and 100 vol % PS at the bottom right. butylated hydroxytoluene (BHT) was added to these blends to prevent thermally crosslinking samples. Comparing the phase behavior of these two different systems, 30/70 through 60/40 blends have drastically different nanostructures.

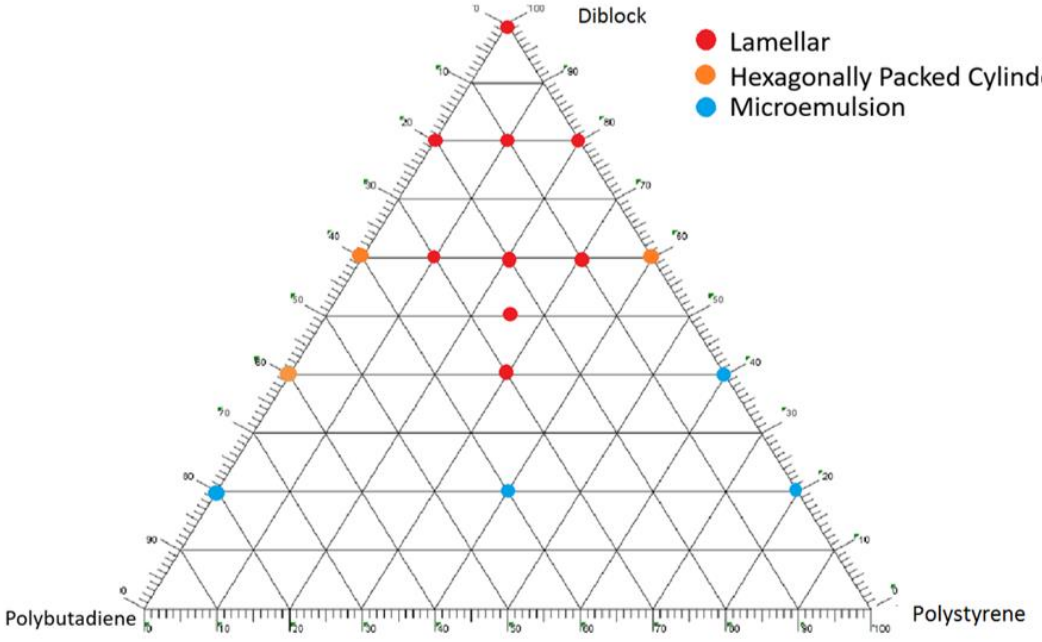

Figure 13. Blends of PS-PBD (diblock), PS, and PBD. All polymers were synthesized via anionic polymerization and blended by freeze drying in benzene, pressing into films, and annealing overnight under dynamic vacuum. Microemulsion is DIS spheres.

Though the volume fractions of polystyrene for the in situ samples are slightly less than the initial volume fractions of styrene present, as the reaction goes to approximately 70% yield, the phase behavior differs greatly and suggests that another factor is changing the phase behavior of PS-PBD/PS blends.

3.3 Grafting in Polymerized PS-PBD/ Styrene Blends

SEC was run for all polymerization-induced samples to determine if the in situ polymerization method had caused any microstructural changes to the initial PS-PBD diblock copolymer. Figure 14 shows representative SEC chromatograms for all blends synthesized. The PS-PBD in Figure 14 was reprecipitated from pressed films and shows a high molecular weight hump. This large molecular weight species is attributed to some crosslinking and has been shown to have no measurable effect on the nanostructures achieved by the polymerization-induced method. After polymerization of the PS-PBD/Styrene blends, a perceptible shift in the PS-PBD SEC trace can be seen toward lower elution times, thus indicating an increase in the molecular weight of the diblock copolymer. This increase in molecular weight was hypothesized to be caused by grafting of styrene onto PS-PBD, yielding PS-PBD-*g*-PS.

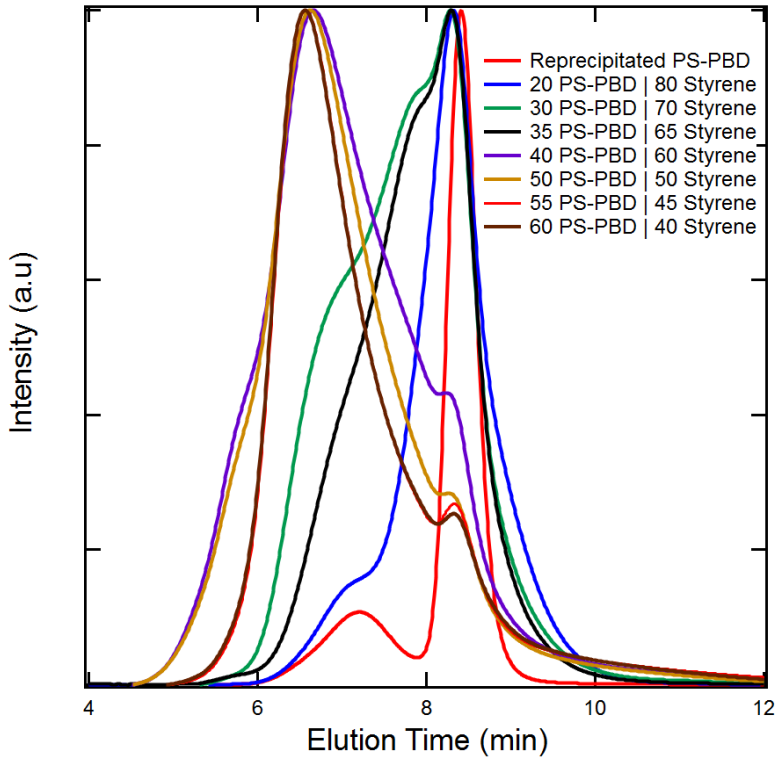

Figure 14. SEC chromatograms for polymerized PS-PBD/Styrene blends.

To ascertain the reason for this increase in molecular weight of PS-PBD after polymerization, PS homopolymer was blended with the styrene/BPO/OH-TEMPO solution and polymerized under identical conditions.

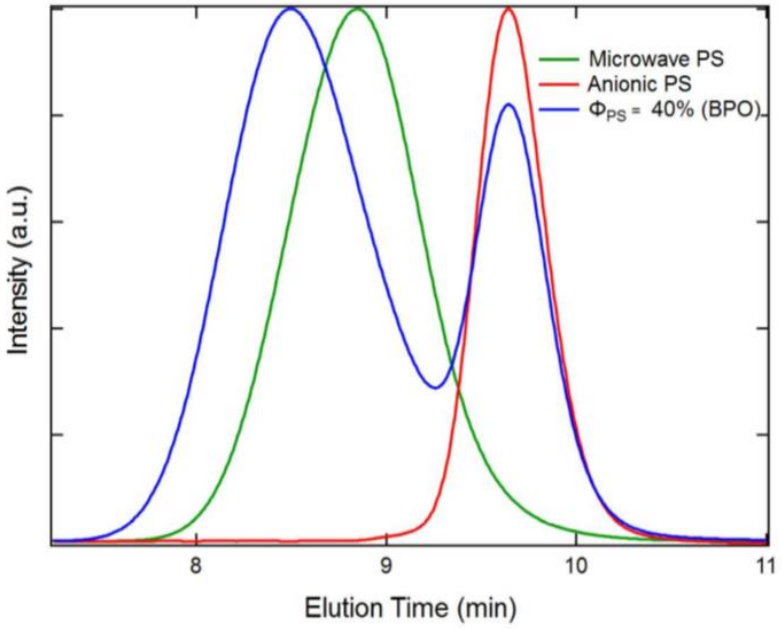

Figure 15. SEC trace for polymerized PS/Styrene blend at ϕ_{PS} = 40%.

No perceptible shift in elution time was observed for the anionically polymerized PS peak in Figure 15. This suggests that no grafting takes place on the PS block of the PS-PBD diblock copolymer, and thus grafting can only occur on the PBD containing block.

The chemical mechanisms proposed for the grafting of PS on the PBD block of PS-PBD are illustrated below in Figure 16. Polystyrene can graft to PBD by either (i) direct attack of a nascent polystyrl chain, (ii) direct attack of an initiator radical, or (iii) abstraction of hydrogen leading to an allylic radical. To determine which chemical mechanism was most dominant in the BPO/OH-TEMPO/Styrene system, PBD with approximately 93% 1,2 content (M_n = 20.3 kg/mol) was blended at 40 vol% with styrene. This volume fraction was chosen because it mimicked the volume fraction of PBD present in 60 PS-PBD/40 Styrene blends.

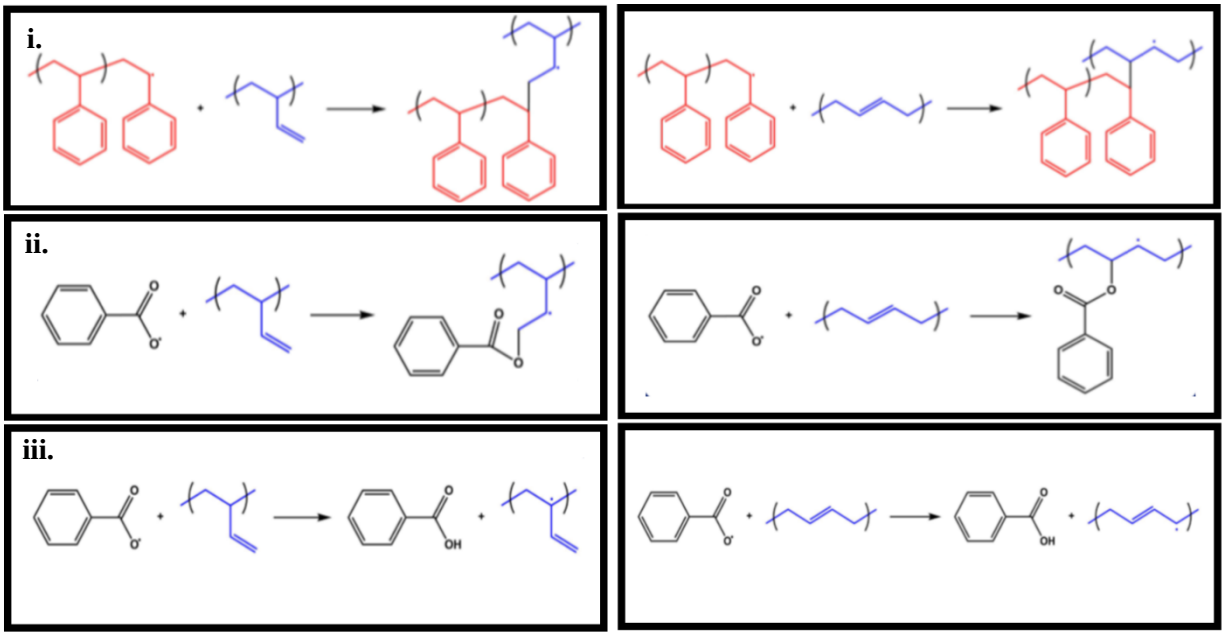

Figure 16. Proposed grafting mechanisms for PBD. From top to bottom are (i) direct attack from polystyrene, (ii) direct attack from a primary radical, and (iii) grafting from an allylic radical. Mechanisms on the left and right are for 1,2PBD and 1,4PBD

Two different initiators, BPO and AIBN, were chosen because BPO can directly attack the PBD backbone or undergo hydrogen abstraction, whereas AIBN can only undergo direct attack of the backbone.[13] If the predominant mechanism is graft-from by hydrogen abstraction, then only the blend containing BPO should undergo appreciable amounts of grafting. The SEC trace in Figure 17 highlights the results of the grafting experiment performed with AIBN and BPO.

From Figure 17, a significant shift toward lower elution times occurs for the BPO containing PBD/styrene blend. On the other hand, a very minimal shift in elution time is observed for the blend containing AIBN as the initiator. Since both AIBN and BPO can undergo primary radical attack and direct attack of nascent polystyrene, the larger shift in elution time for the BPO containing blend can be attributed to mechanism (iii) in which BPO abstracts a hydrogen atom, yielding an allylic radical that can initiate and propagate styrene.[14] Though

hydrogen abstraction appears to be the primary grafting mechanism, it is unclear whether this grafting-from takes place on the 3˚ allylic carbon in 1,2PBD or the 2˚ allylic carbon in 1,4PBD.

Previous synthetic and computational work related to graft copolymers have shown an intricate relationship between phase behavior and the number, length, and density of grafts.[15-21] The work presented in this thesis differs from previous synthetic graft copolymer studies in that the graft parameters are not well controlled and are not easily discernible experimentally. The final volume fraction of polystyrene is one of the few parameters that can be determined with relative ease by determining the increase in mass of the PS-PBD after removal of all unreacted styrene. The final PS content in the PS-PBD-*g*-PS was determined to be $f_{PS} \approx 0.67$, 0.76, and 0.87 for the $\phi_{PS\text{-}PBD}$ = 60%, 40%, and 20% samples, respectively. Further studies are required to ascertain the exact number of PS grafts per PBD block, as the number of grafts in theory should change the final morphology of the PS-PBD-*g*-PS system.[21]

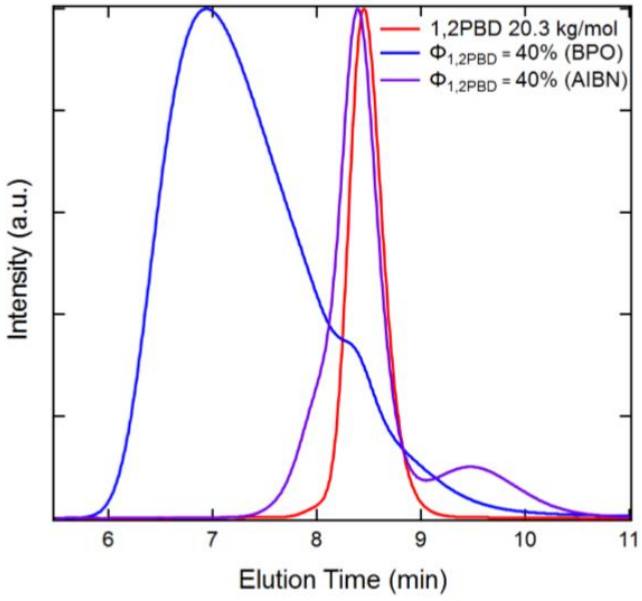

Figure 17. SEC trace for polymerized PBD/Styrene blend at ϕ_{PBD} = 40%

Chapter 4: In Situ Monitoring of Nanostructural Transitions

4.1 Phase Behavior of Block Copolymer in Neutral Solvents

The phase behavior of BCPs swollen with solvent has been extensively studied due to the frequency with which they are combined in applications. Solvents can be characterized as either selective or neutral with respect to the BCP they are swelling. In the case of a selective solvent, a single block is preferentially swollen, while in a neutral solvent both blocks are swollen evenly.[22] Additionally, a solvent can be further classified as good, neutral, or theta. In the case of a good solvent, the interactions between the polymer repeat units and the surrounding solvent are more favorable than the interactions between individual repeat units with themselves, causing chains to extend beyond their gaussian coil conformation. On the other hand, a bad solvent is present when the repeat units within a chain interact with each other more favorably than with the surrounding solvent, subsequently leading to a smaller R_g and end-to-end distance for the macromolecule relative to the melt. Lastly, a theta solvent (theta condition) exists when interactions between repeat units and solvent are sufficient such that they precisely counteract chain expansion due to excluded volume, allowing the chain to adopt a random walk conformation.

Generally speaking, neutral solvent swelling dilutes the interactions between the A and B repeat units in diblock copolymers. Dilution with solvent subsequently suppresses the OOT, ODT, and glass-transition temperatures of a BCP, thus significantly impacting the mesoscale order of the material.[22] These decreases in temperature are generally accounted for by a decrease in χ to a new value, χ_{eff}. This naturally causes new phase behavior to arise in the system due to a dilution of the enthalpic interaction between A and B repeat units.

In many cases, the simple dilution approximation of $\chi_{eff} \sim \varphi\chi$ can be used, where φ is the volume fraction of diblock copolymer.[22] This approximation describes OOTs remarkably well, yet consistently fails for ODTs, specifically for LAM to DIS ODTs. Additionally, experiments suggest that χ_{eff} behavior is not universal.[22] The complex phase behavior of BCPs swollen with solvent contributes to the fascinating phase behavior observed during polymerization-induced nanostructural transitions, particularly for $\phi_{PS\text{-}PBD}$ = 60% blends.

4.2 In Situ SAXS Characterization of Morphology Transitions

In situ SAXS experiments were performed to provide further insight into the process by which $\phi_{PS\text{-}PBD}$ = 60% transitions from LAM to HEX during grafting and polymerization. The $\phi_{PS\text{-}PBD}$ = 60% blend was prepared using previously established methods, loaded into capillary tubes, and sealed with epoxy to prevent loss of styrene by evaporation over time. Samples were heated on a Linkam stage to 125 °C and periodically scanned to reveal the nanostructure as a function of reaction progress.

Both blocks of PS-PBD are initially swollen by styrene, which acts as a neutral solvent that partitions evenly between PS and PBD. The $\phi_{PS\text{-}PBD}$ = 60% blend was scanned for 5 mins and revealed a symmetric LAM morphology, as suggested by the absence of evenly indexed peaks. The sample was then heated on the Linkam stage from 25 °C to 125 °C. During heating, polymerization and grafting are initiated simultaneously, while the χ decrease associated with the increase in temperature drives the block copolymer to disorder.

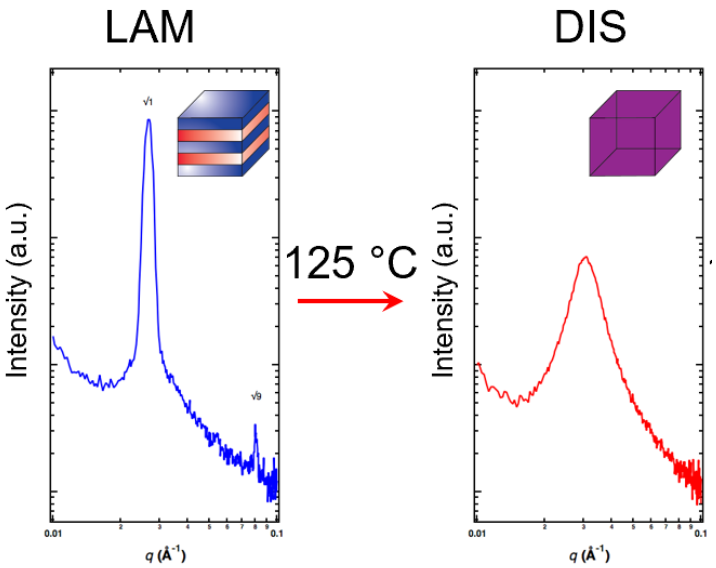

Figure 18. SAXS pattern showing disordering of $\phi_{PS\text{-}PBD}$ = 60% at 125 °C

Immediately after reaching 125 °C, scans of the blend showed a shift in the primary peak toward higher q, a broadening of the primary peak accompanied by an order of magnitude decrease in scattering intensity, and annihilation of higher order reflections, all of which are indicative of disordering. The role that disordering plays in the final nanostructure achieved after polymerization is still an open question that must be addressed to provide a deeper understanding of the physical mechanisms taking place during polymerization-induced nanostructural transitions. After approximately 10 minutes of heating, a sharp primary peak, q^*, begins to develop, as shown in Figure 19. The dramatic increase in scattering intensity and decrease of the full width at half maximum of q^* indicates some transition from a disordered to an ordered state, yet the absence of any higher order reflections makes it impossible to discern the ordered structure observed by SAXS. In this state, the material likely lacks any long-range order, or is coarsely ordered. Further analysis may be helpful in determining the nanostructure observed after ordering, such as TEM or atomic force microscopy (AFM), but this characterization is beyond the scope of this thesis.

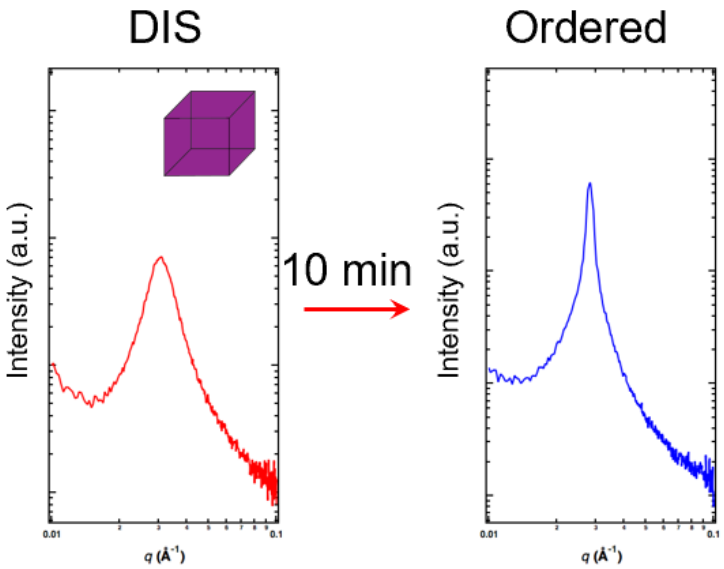

Figure 19. SAXS showing a transition from disorder to order after 10 minutes at 125 °C

The primary scattering peak that appears after 10 mins at 125 °C persists for over 1 h of reaction time. During this time, q^* shifts toward lower q and the full-width at half maximum decreases. Two processes are thought to be occurring simultaneously: (1) monomer is being depleted, leading to an increase in the overall volume fraction of PS-PBD in the blend and thus an increase in χ_{eff}, and (2) grafted and homopolymer PS are being formed, leading to an increase in the degree of polymerization, N. These two simultaneous events lead to the incredibly complicated and intricate phase behavior observed in the system.

At 90 min, the SAXS reveals new higher order reflections near q^*, which can be indexed as $\sqrt{6}$ and $\sqrt{8}$, respectively. This indexing is indicative of a gyroid (GYR) nanostructure, a morphology that is notoriously difficult to nucleate and has received much interest for its potential applications.[23] Over the remaining 1.5 h of reaction time, the coarse gyroid becomes more refined, garnering higher order reflections that are indicative of long-range structure.

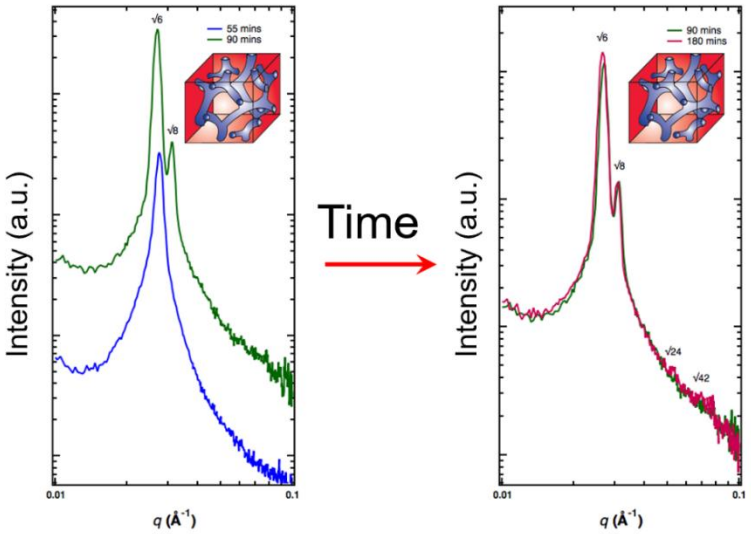

Figure 20. 1D SAXS pattern illustrating the evolution of an ordered morphology to gyroid a gyroid structure, and the evolution of gyroid as the reaction proceeds.

Upon cooling, the blend transitions from GYR to HEX. As temperature decreases, the √8 peak diminishes in intensity until it is no longer present. Additionally, the *q* value of the √24 and √42 peaks is identical to the *q* associated with the √4 and √7 peaks in HEX, as shown in Figure 21.

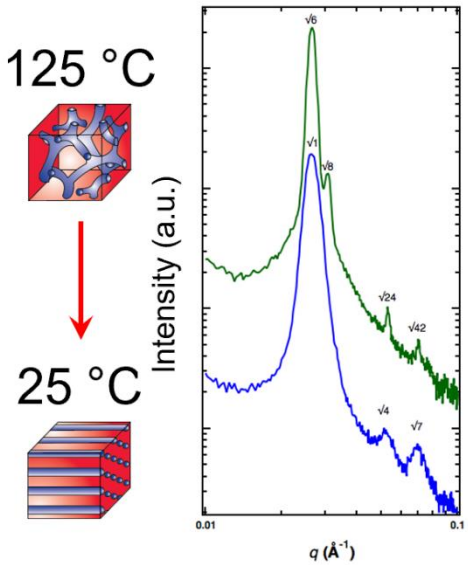

Figure 21. 1D SAXS pattern showing the reversible transition from GYR to HEX upon cooling

4.3 Comparison of In Situ SAXS and Rheology

Rheology is the study of the elastic and viscous response of materials, such as polymers, to shear or strain. The viscoelastic response of a polymer to a mechanical perturbation depends on many underlying factors, including the nanoscale structure, temperature, and the rate of deformation applied to the material. The solid response of a material, encapsulated by the storage modulus (G'), is indicative of the elasticity of a material, or how well it can reversibly store mechanical energy. The loss modulus (G'') on the other hand describes how a material irreversibly dissipates a mechanical perturbation through viscous flow. By probing the elastic and viscous response of a polymer melt via rheology, a plethora of information regarding the nanoscale morphology of a material can be observed, including OOT and ODT.

Approximately 0.1 mL of $\phi_{PS\text{-}PBD}$ = 60% blend was loaded onto 8 mm diameter parallel plates in an ARES G2 rheometer (Rheometrics). The sample was sheared to a uniform thickness and purged of all air bubbles. Strain sweeps were performed ranging from 0.1 to 1% to ensure a linear mechanical response over the range of strain applied. A frequency sweep was performed between 0.1 and 100 rad/s and the storage and loss moduli recorded, as shown in Figure 22. The approximate slope of ½ from the Log-Log plot is a universal response of LAM forming diblock copolymers, and is thus a verification of the LAM scattering pattern observed previously.[24]

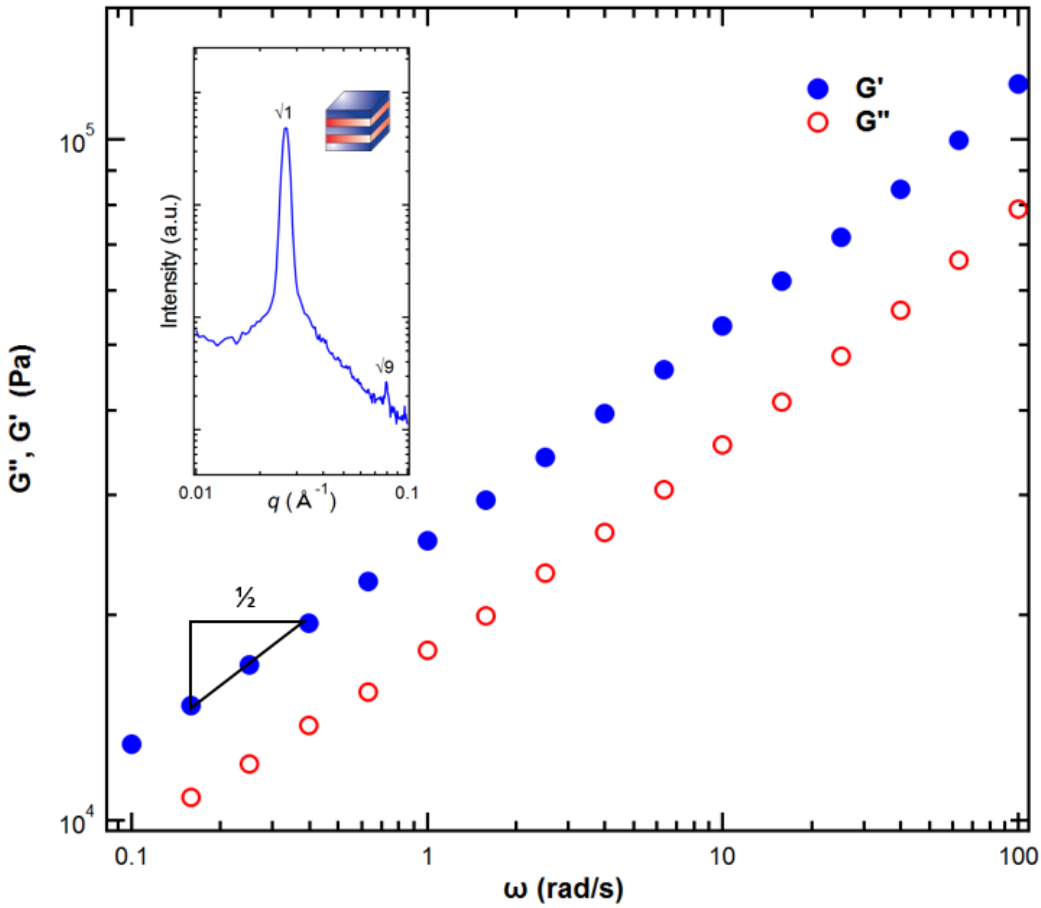

Figure 22. Room temperature frequency sweep for $\phi_{PS\text{-}PBD}$ blend and corresponding SAXS. The slope of ½ suggest a LAM morphology, as confirmed by the inset scattering pattern.

The storage and loss moduli were next monitored as the temperature was increased from 25 °C to 125 °C. As temperature increases, the storage and loss modulus of the sample both decrease as the blend softens. Figure 23 shows the temperature ramp for $\phi_{PS\text{-}PBD}$ = 60%. Between 40 and 60 °C the moduli plateau, an observation that may correspond to an OOT, though SAXS must be run to confirm this hypothesis. Near 80 °C the moduli response becomes noisy, indicating that the sample has either transitioned from LAM to DIS, or the torque fell below the minimum threshold of the rheometer's transducer.

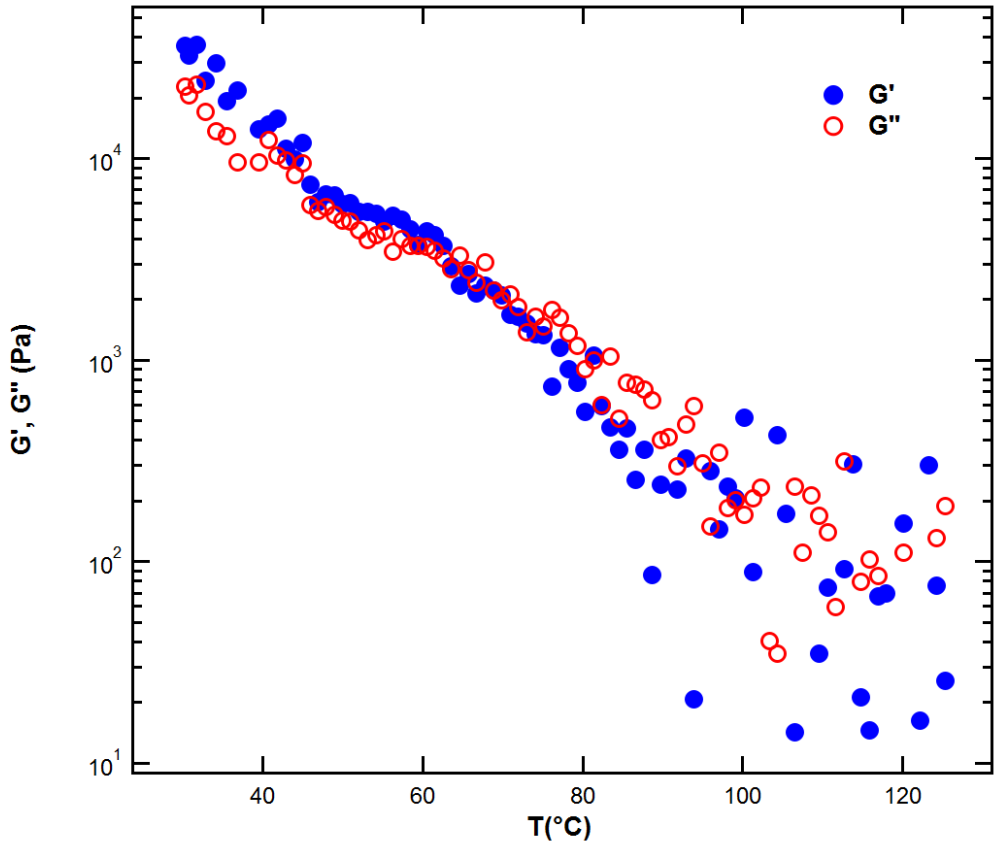

Figure 23. Temperature ramp for $\phi_{PS\text{-}PBD}$ = 60% sample

After reaching 125 °C, an isothermal time sweep was performed for 3 h. Initially, the loss modulus is larger than the storage modulus and both moduli rapidly increase with time. Figure 24 shows that approximately 10 min into the reaction, the loss and storage moduli cross and the increase in modulus with respect to time drastically decreases. The crossover where G' > G'' aligns almost exactly with the disorder to order transition observed in the in situ SAXS experiment. After the crossover at 10 min, no other major changes in modulus can be seen. If a second order-order transition to GYR were present, one would expect an abrupt increase in modulus; however, no perceptible increase in modulus is observed after 1 h, suggesting that the

ordered morphology obtained after 10 mins is a coarse gyroid structure that becomes more refined over time.[24]

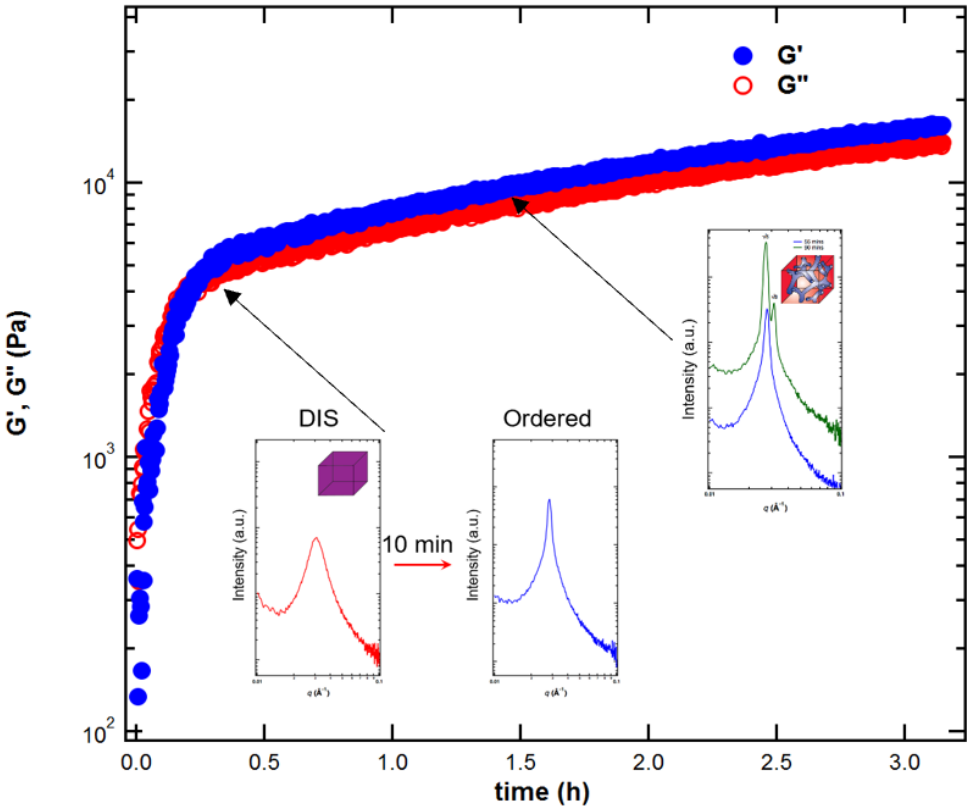

Figure 24. Isothermal (125 °C) time sweep for $\phi_{PS\text{-}PBD}$

After completing the 3 h reaction, a frequency sweep was performed at 0.5 % strain and 125 °C. At low frequency, the loss modulus dominates the storage modulus. The opposite trend is observed at higher frequencies, with a crossover occurring around 6 rad/s. At low frequencies, GYR forming diblock and triblock copolymers exhibit a crossover reminiscent of that shown in Figure 25.[24] The frequency sweep at 125 °C after polymerization as well as the SAXS together confirm that at 125 °C the gyroid structure is present.

A frequency sweep was also performed at 70 °C with a 0.5% strain rate and is shown in Figure 26. The slope of G' and G'' was found to be 0.23, which is approximately the scaling relationship of ~1/3 that is expected for HEX forming BCPs. More importantly, the frequency response of the moduli are drastically different between the 125 °C and 70 °C sweeps, suggesting different nanostructures are present at these two temperatures.

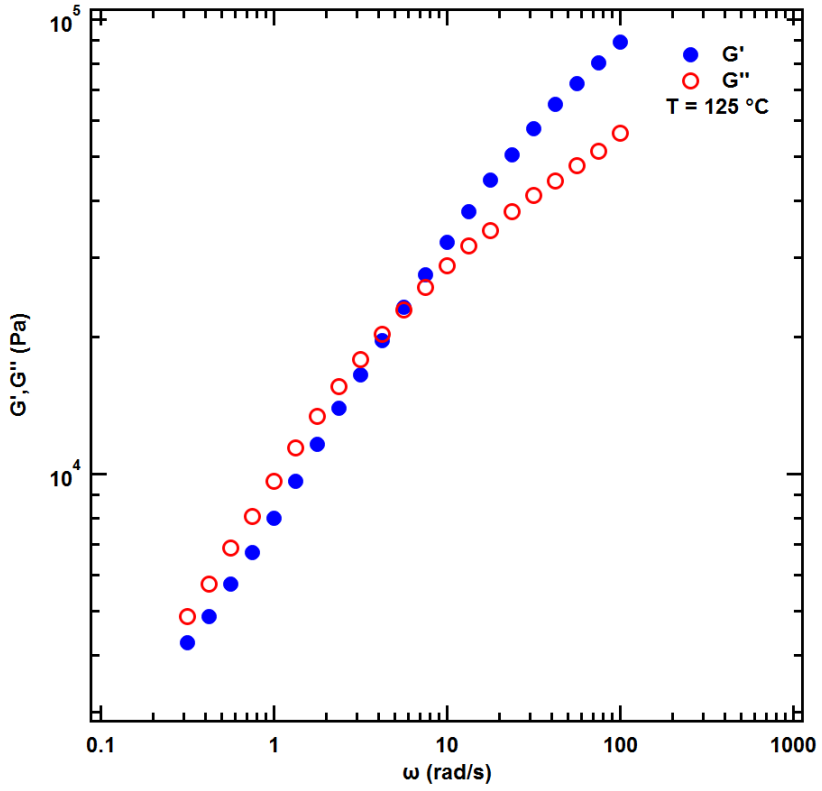

Figure 25. Frequency sweep performed on $\phi_{PS\text{-}PBD}$ = 60% 0.5% strain and 125 °C

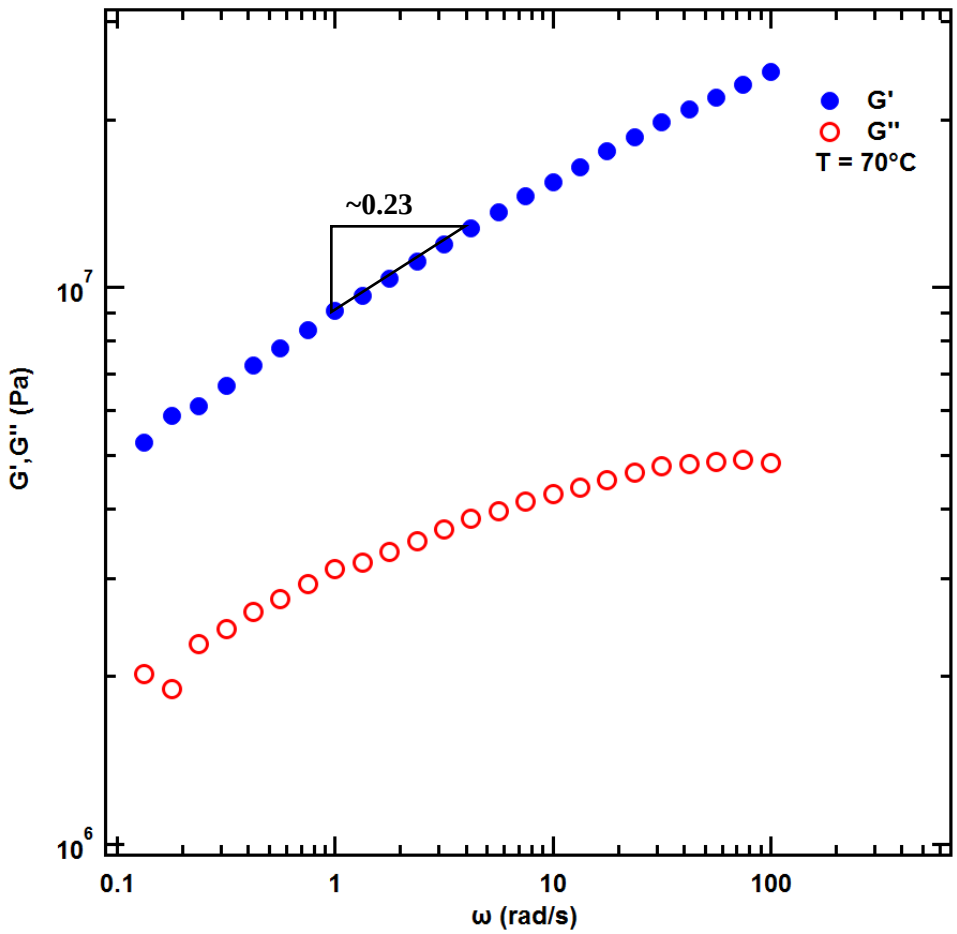

Figure 26. Frequency sweep performed at 70 °C for $\phi_{PS\text{-}PBD}$ = 60% at 0.5% strain. The slope of 0.23 is close to the approximate 0.33 slope required for HEX.

The storage and loss moduli of the $\phi_{PS\text{-}PBD}$ = 60% sample post-polymerization were monitored during a temperature sweep from 125 °C to 35 °C and the data is presented in Figure 27. From SAXS, the transition from GYR to HEX occurs somewhere near 70 and 80 °C and persists until approximately 60 °C. The rheology data appears to have a sharp deviation between G' and G'' between 70 and 95 °C, which aligns well with the SAXS data. During the SAXS cooling experiments, only 5 minutes was allotted between each scan, which may not be enough time for the PS-PBD-g-PS to molecules to diffuse into their thermodynamic nanostructures (graft-copolymer melts and solutions are highly viscous, hence their use as viscosity modifiers).

Thus, the experiment may under-approximate the OOT temperature; however, the rheological experiment was run at a cooling rate of 5 °C/min, which may also lead to an under-approximation of the OOT temperature. Nevertheless, the rheology appears to show deviations in storage and loss moduli near temperatures where SAXS suggests transitions are occurring.

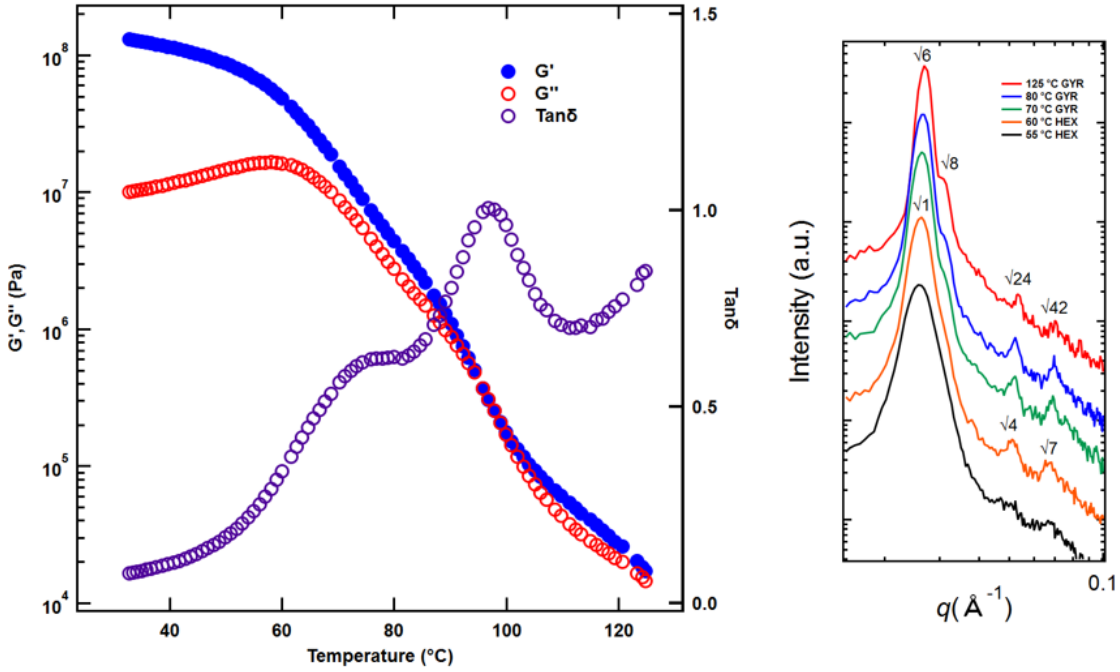

Figure 27. SAXS and rheology data on cooling from 125 °C. SAXS suggest that the OOT occurs near 70 °C, and is accompanied by a deviation of G'' from G' on rheology

Tanδ, which is defined as the ratio of the loss and storage moduli, is plotted on the right axis in Figure 27. Typically, tanδ is at a maximum when the material goes through glass-transition; however, the trends for G'' and G' in Figure 27 are not characteristic of glass transition.

Typically, at $T >> T_g$ the loss modulus dominates the storage modulus and the material behaves as a viscous liquid. At $T > T_g$, the two moduli will plateau. This region is called the "rubber plateau" and occurs somewhere between terminal viscous flow and the glass transition. When $T \approx T_g$, G'' and G' drastically increase with G' > G''. When $T \leq T_g$, the two moduli plateau again with G' > G''. Given this information, it is possible that between 40 and 60 °C the

blend is behaving as an entangled rubber, or the blend is approaching its glass-transition. From DSC (Figure 28), the T_g of the blend appears to be near 20 °C, which would support the hypothesis that the rubber plateau is being observed between 40 and 60 °C. The T_g is identified by DSC via the inflection in the heat flow curve.

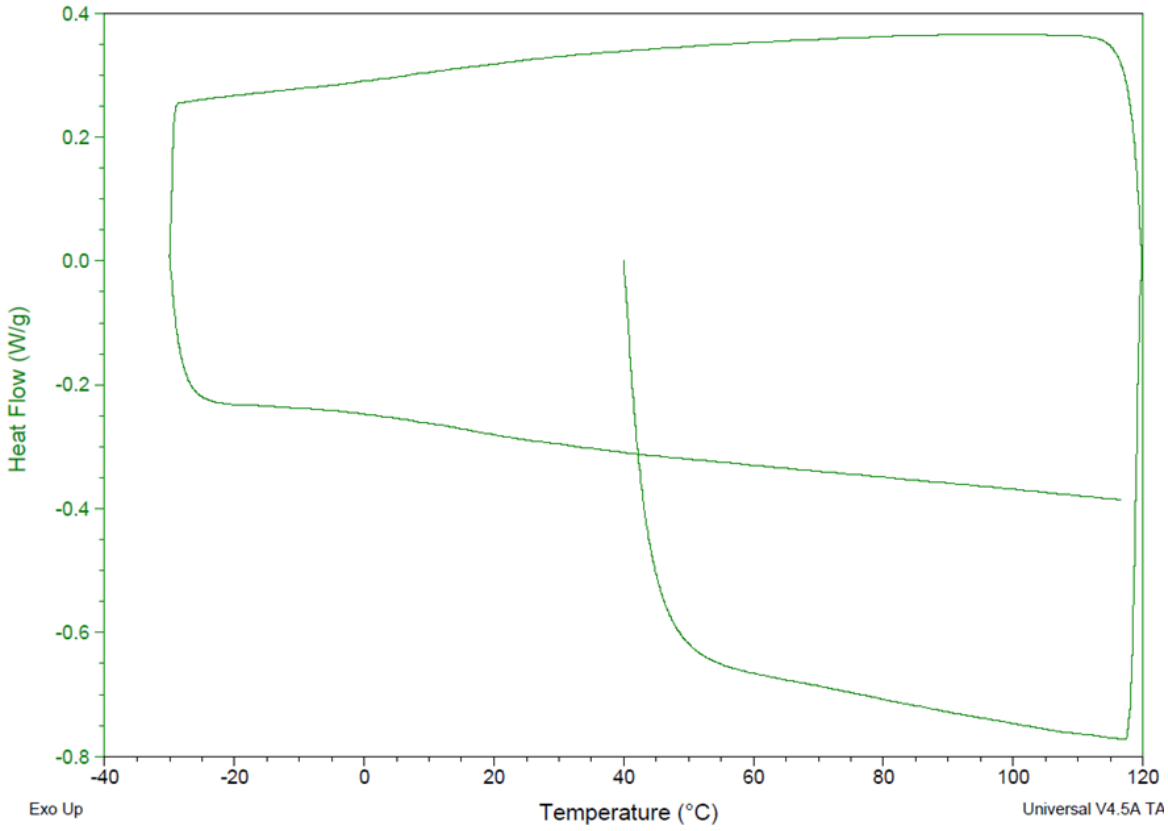

Figure 28. DSC trace for $\phi_{PS\text{-}PBD}$ = 60% run at a heating rate of 10 °C/min.

Since the T_g is sub-ambient, the GYR structure cannot be retained after rapidly quenching from 125 °C to room temperature. Since GYR is a technologically relevant nanostructure, it would be ideal if one could obtain the structure via rapid quenching to room temperature, followed by evacuation of styrene under dynamic vacuum. To achieve this, longer reactions should be attempted, leading to larger styrene conversion and thus a higher T_g. Once the T_g of the post-polymerization blend is greater than room temperature, the GYR structure can be

kinetically trapped, allowing for the facile synthesis of a technologically important nanostructure.

Chapter 5: Conclusions

In summary, the work outlined in this thesis has explored the phase behavior, both static and in situ, of nanostructured polymeric materials synthesized via polymerization induced nanostructural transitions. In this method, PS-PBD was synthesized via living anionic polymerization, blended with a solution of styrene, OH-Tempo, and BPO in various volume fractions, and polymerized for 3 h. The resulting blends were characterized via SAXS and TEM and revealed interesting nanostructural transitions from DIS and LAM to DIS spheres, HEX, and LAM. SEC experiments revealed that PS grafts from PS-PBD during the reaction. Grafting experiments were then performed on PS and PBD homopolymer to determine where PS grafting occurs during in situ polymerization. Grafting was determined to occur from the PBD block of PS-PBD, and AIBN and BPO grafting studies were performed to provide insight into the chemical mechanism at play. These grafting studies suggest that PS is grafted from PBD via a hydrogen abstraction mechanism, though it is unknown whether 1,4 or 1,2 PBD yields better grafting.

In situ SAXS experiments were performed on $\phi_{PS\text{-}PBD}$ = 60% blends on a temperature-controlled stage. In situ studies showed that at 125 °C, the blend transitions from LAM to DIS, and then subsequently reorders after 10 mins of reaction time. Though the blend orders after 10 mins, no higher order reflections are present in the 1D SAXS pattern and the structure therefore cannot be determined. After 1.5 h of polymerization, higher order peaks appear on the 1D SAXS

pattern that indexed to GYR. Over time, the GYR structure becomes more refined and more higher order reflections can be indexed. Upon cooling to 25 °C the morphology was indexed as HEX.

Rheology was used to confirm the observations made via SAXS. A time sweep showed that after 10 mins of reaction the magnitude of the storage modulus is greater than the loss modulus, which coincided with the ordering observed by SAXS. No other drastic increase in moduli were observed, which suggested that the ordered structure observed after 10 min of reaction was a coarse gyroid that became more refined over time. Frequency sweeps at 125 °C and 70 °C showed moduli responses that were reminiscent of GYR and HEX, respectively. A temperature ramp from 125 °C to 30 °C showed that the storage and loss moduli deviate from one another between 90 °C and 70 °C, which coincided with the transition between GYR and HEX observed in SAXS.

BIBLIOGRAPHY

1. Karagoz, B.; Esser, L.; Duong, H. T.; Basuki, J. S.; Boyer, C.; Davis, T. P. *Polym. Chem.* **2014**, *5* (2), 350–355.

2. Schulze, M. W.; Mcintosh, L. D.; Hillmyer, M. A.; Lodge, T. P. *Nano Letters* **2013**, *14* (1), 122–126.

3. Sardelis, K.; Michels, H. J.; Allen, G. Toughened Polystyrene Containing Block, Graded Block and Randomized Copolymers of Butadiene-Styrene. Polymer **1987**, 28, 244−250.

4. Leal, G. P.; Asua, J. M. Evolution of the Morphology of Hips Particles. Polymer **2009**, 50, 68−76.

5. Meira, G. R.; Luciani, C. V.; Estenoz, D. A. Continuous Bulk Process for the Production of High-Impact Polystyrene: Recent Developments in Modeling and Control. Macromol. React. Eng. **2007**, 1, 25−39.

6. Bates, C. M.; Bates, F. S. 50th Anniversary Perspective: Block Polymers - Pure Potential. Macromolecules **2017**, 50,3−22.

7. Bates, F. S. Science **1991**, *251*(4996), 898–905.

8. Ndoni, S.; Papadakis, C. M.; Bates, F. S.; Almdal, K. Laboratory-Scale Setup for Anionic Polymerization under Inert Atmosphere. Rev. Sci. Instrum. **1995**, 66, 1090-1095.

9. Mansour, A. S.; Johnson, L. F.; Lodge, T. P.; Bates, F. S. Thermodynamic Characteristics of Poly(Cyclohexylethylene-b-Ethylene-co-Ethylethylene) Block Copolymers. J. Polym. Sci. B **2010**, 48, 566-574.

10. Delaittre, G. *Nitroxide Mediated Polymerization Polymer Chemistry Series* 199–263.

11. Leibler, L. *Macromolecules* **1980**, *13*(6), 1602–1617.

12. Honda, T.; Kawakatsu, T. *Macromolecules* **2006**, *39* (6), 2340–2349.

13. Huang, N. J.; Sundberg, D. C. Fundamental Studies of Grafting Reactions in Free Radical Copolymerization. Iv. Grafting of Styrene, Acrylate, and Methacrylate Monomers onto Vinyl-Polybutadiene Using Benzoyl Peroxide and Aibn Initiators in Solution Polymerization. *J. Polym. Sci., Part A: Polym. Chem*. **1995**, 33, 2587−2603.

14. José, B. C.; Enrique, S. G.; Román, T. L. J.; Ramiro, G. S.; Bruno, L. C.; Gabriel, L. B. Controlled Grafting-from of Polystyrene on Polybutadiene: Mechanism and Spectroscopic Evidence of the Functionalization of Polybutadiene with 4-Oxo-Tempo. Macromol. *Chem. Phys.* **2008**, 209, 2268−2283

15. Beyer, F. L.; Gido, S. P.; Büschl, C.; Iatrou, H.; Uhrig, D.; Mays, J. W.; Chang, M. Y.; Garetz, B. A.; Balsara, N. P.; Tan, N. B.; Hadjichristidis, N. Graft Copolymers with Regularly Spaced, Tetrafunctional Branch Points: Morphology and Grain Structure. *Macromolecules* **2000**, 33, 2039−2048.

16. Xenidou, M.; Beyer, F. L.; Hadjichristidis, N.; Gido, S. P.; Tan, N. B. Morphology of Model Graft Copolymers with Randomly Placed Trifunctional and Tetrafunctional Branch Points. *Macromolecules* **1998**, 31, 7659−7667.

17. Zhang, L.; Lin, J.; Lin, S. Effect of Molecular Architecture on Phase Behavior of Graft Copolymers. *J. Phys. Chem. B* **2008**, 112, 9720−9728

18. Hart, K. E.; Abbott, L. J.; Lísal, M.; Colina, C. M. Morphology and Molecular Bridging in Comb- and Star-Shaped Diblock Copolymers. *J. Chem. Phys*. **2014**, 141, 204902.

19. Qi, S.; Chakraborty, A. K.; Balsara, N. P. Microphase Segregation in Molten Randomly Grafted Copolymers. *J. Chem. Phys.* **2001**, 115, 3387−3400.

20. Qi, S.; Chakraborty, A. K.; Wang, H.; Lefebvre, A. A.; Balsara, N. P.; Shakhnovich, E. I.; Xenidou, M.; Hadjichristidis, N. Microphase Ordering in Melts of Randomly Grafted Copolymers. *Phys. Rev. Lett*. **1999**, 82, 2896−2899.

21. Milner, S. T. Chain Architecture and Asymmetry in Copolymer Microphases. *Macromolecules* **1994**, 27, 2333−2335.

22. Lodge, T. P.; Hanley, K. J.; Pudil, B.; Alahapperuma, V. *Macromolecules* **2003**, *36* (3), 816–822.

23. Kumar, A.; Molinero, V. *The Journal of Physical Chemistry B* **2018**, *122* (17), 4758–4770.

24. Kossuth, M. B.; Morse, D. C.; Bates, F. S. *Journal of Rheology* **1999**, *43* (1), 167–196.

25. http://web.mit.edu/8.334/www/grades/projects/projects10/AlexanderPapageorge/Page6.html (accessed Apr 4, 2019).

Everett S. Zofchak
The Pennsylvania State University

Schreyer Honors College | B.S Chemical Engineering | 07/15 – 05/19

B.S Materials Science & Engineering

Fellowships and Awards

PMSE Best Poster Award, ACS National Meeting in Boston, 2018
Erickson Discovery Grant, Pennsylvania State University, Pennsylvania State University,2018
Broughton Trustee Scholarship in Engineering, Pennsylvania State University, 2018-19
Society of Distinguished Alumni Scholarship, Pennsylvania State University, 2017-18
Penn State Academic Grant, 2017-2019
Penn State Research Scholarship 2017
PPG Materials Research Institute Fellowship, Pennsylvania State University, 2017
Dean's List, Pennsylvania State University, 2015-2018

Publications

1.) E.S. Zofchak, J.A. Lanasa, W. Mei, R.J. Hickey, "Polymerization-Induced Nanostructural Transitions Driven by in situ Polymer Grafting", ACS Macro Lett., 2018, 7, 822.
2.) E.S. Zofchak, Honors Undergraduate Thesis "Polymeriztion-Induced Nanostructural Transitions Driven by in situ Polymer Grafting for Diblock Copolymer and Monomer Blends"

Oral Presentations

1.) E.S. Zofchak "Synthesis, Characterization, and Mechanical Properties of Nanostructured High Impact Polystyrene" 2017 PPG/ MRI Fellowship Presentation at PPG R&D Headquarters, Allison Park, PA, July 27, 2017. (Invited)

Poster Presentations

1.) E.S Zofchak "Polymerization Induced order-order and disorder-order Transitions in Diblock Copolymer/Monomer Blends" Materials Day Presentation, State College, PA, Oct. 24 2018
2.) E.S Zofchak "Polymerization Induced order-order and disorder-order Transitions in Diblock Copolymer/Monomer Blends" ACS National Conference, Boston, MA, August 21, 2018.
3.) E.S Zofchak, B. Garland, K. Bah, C. Zhang, and M. Qutub "Solid State Li-ion Polymer Batteries for High Temperature Applications", State College, PA, March 21, 2018
4.) E.S. Zofchak "Synthesis, Characterization, and Mechanical Properties of Nanostructured High Impact Polystyrene" Undergraduate Research Exhibition, The Pennsylvania State University, State College, PA, July 2017

Teaching and Work Experience

Calculus I & II "Orals" Learning Assistant: 08/16 – Present

Led problem-solving sessions for groups of 4-6 Math 140/141 students through the Mathematics department at Penn State. Tracked multiple students' work, anticipated mistakes, and helped them correct their errors through only oral communication.

Intern at Envirotek Laboratories: 05/16 – 09/16

Tested the efficacy of claims made by water filter manufacturers. Created large solutions of organic, inorganic, and bacterial contaminants, passed them through filters, and determined contaminant concentrations in the effluent.

Intern at Ocean Environmental Laboratories: 06/14 - 01/15

Analyzed commercial and residential water for organic and inorganic contaminants using GC-MS and plasma atomic emission spectroscopy. Interfaced with customers to provide results of water tests and trained new interns on experimental procedures.